IOP Publishing Physiol. Meas. 40 (2019) 095007 (12pp) https://doi.org/10.1088/1361-6579/ab3be0

Physiological Measurement

IPEM Institute of Physics and Engineering in Medicine

PAPER

Finger and forehead PPG signal comparison for respiratory rate estimation

RECEIVED
8 April 2019

REVISED
5 August 2019

ACCEPTED FOR PUBLICATION
16 August 2019

PUBLISHED
27 September 2019

A Hernando[1,2,4], M D Peláez-Coca[1,2], M T Lozano[1,2], J Lázaro[2,3,4] and E Gil[2,4]

[1] Centro Universitario de la Defensa (CUD), Academia General Militar (AGM), Zaragoza, Spain
[2] BSICoS Group, Aragón Institute of Engineering Research (I3A), IIS Aragón, University of Zaragoza, Zaragoza, Spain
[3] Department of Biomedical Engineering, University of Connecticut, Storrs CT, United States of America
[4] Centro de Investigación Biomédica en Red - Bioingeniería, Biomateriales y Nanomedicina (CIBER-BBN), Madrid, Spain

E-mail: ahersanz@unizar.es

Keywords: PPG, finger, forehead, respiratory rate estimation

Abstract

Objective: An evaluation of the location of the photoplethysmogram (PPG) sensor for respiratory rate estimation is performed. *Approach*: Finger PPG, forehead PPG, and respiratory signal were simultaneously recorded from 35 subjects while breathing spontaneously, and during controlled respiration experiments at a constant rate from 0.1 Hz to 0.6 Hz, in 0.1 Hz steps. Four PPG-derived respiratory (PDR) signals were extracted from each one of the recorded PPG signals: pulse rate variability (PRV), pulse width variability, pulse amplitude variability and the respiratory-induced intensity variability (RIIV). Respiratory rate was estimated from each one of the four PDR signals for both PPG sensor locations. In addition, different combinations of PDR signals, power distribution of the respiratory frequency range and differences of the morphological parameters extracted from both PPG signals have been analysed. *Main results*: Results show better performance in terms of successful estimation and relative error when: (i) PPG signal is recorded in the finger; (ii) the respiratory rate is less than 0.4 Hz; (iii) RIIV signal is not considered. Furthermore, lower spectral power around the respiratory rate in the PDR signals recorded from the forehead was observed. *Significance*: These results suggest that respiratory rate estimation is better at lower rates (0.4 Hz and below) and that the finger is better than the forehead to estimate respiratory rate.

1. Introduction

The pulse photoplethysmographic (PPG) signal is a non-invasive technique widely used to obtain clinic monitoring information (Shelley 2007, Seymour *et al* 2010). This technique was explained for first time by Hertzman and Spielman (1937), and has usually been used to detect blood volume changes in the microvascular bed of tissue (Challoner and Ramsay). Currently, PPG measurement needs only one low-cost device widely used in the clinical routine that can be located in several parts of the body. Among its multiple applications, the most highlighted are (Allen 2007) the following: evaluation of the autonomic nervous system (ANS) through pulse rate variability (Nitzan *et al* 1998, Gil *et al* 2010); vascular assessment, measuring the arterial disease, compliance or ageing among others characteristics of the vascular tissue (Takazawa *et al* 1998); and the physiological monitoring of the organism, estimating the heart rate and the oxygen saturation (Jensen *et al* 1998, Chon *et al* 2009).

Analysis of the pulse photoplethysmographic waveform also offers a non-invasive alternative for respiratory rate monitoring based on the assumption that respiration modulates the PPG signal through several effects (Meredith *et al* 2012). Many works have developed algorithms to estimate the respiratory rate from the PPG signal directly, as in Chon *et al* (2009), where the respiratory rate is estimated using time-frequency spectral methods, or in Lin *et al* (2013), where autoregressive decomposition is applied. Authors of other works prefer to develop their algorithms over PPG-derived respiration (PDR) signals, which reflect respiratory modulation over the PPG. Probably the most common PDR signal used to extract the respiratory information is the respiratory-induced intensity variability signal (RIIV) (Nilsson *et al* 2000, Karlen *et al* 2013, Lin *et al* 2013). This modulation arises from respiratory-induced variations in venous return to the heart, caused by the alterations

in intrathoracic pressure. Other possible PDR signals described in the literature are: pulse rate variability (PRV), modulated by respiration through respiratory sinus arrythmia (Dash *et al* 2010); pulse amplitude variability (PAV), also modulated by respiration through variations in stroke volume and in blood vessels stiffness (Johansson and Oberg 1999); and pulse width variability (PWV), modulated by blood vessels stiffness in addition to the pressure changes in the thorax during the respiratory cycle (Lázaro *et al* 2013). Respiratory rate estimation can be done over one of these PDR signals or over an ensemble of them, through the application of several techniques such as the fusion of fast Fourier transforms (Karlen *et al* 2013), wavelet transform methods (Addison *et al* 2015) or peak-averaged combination of power spectra estimation (Lázaro *et al* 2013).

All the mentioned works have one thing in common: the PPG sensor is located in the finger. However, morphological changes in PPG have been observed due to the location in the body where the PPG is registered (Allen 2007, Hartmann *et al* 2019) and due to different respiratory patterns such as deep or spontaneous breathing (Hartmann *et al* 2019). Even more, the PPG signal spectral power in the respiratory band is also affected by the PPG sensor location (Nilsson *et al* 2007). A few works in the bibliography have compared respiratory rate estimations extracted from different PPG locations, as in Johnston and Mendelson (2004), where the finger and forehead were compared and good results were obtained in both locations, or in Charlton *et al* (2017), where the finger was chosen as the best place to locate the PPG sensor. However, these works do not explore the reasons why performance at these locations is different. Therefore, we propose a deep study comparing the respiratory rate estimation of two possible PPG sensor locations, together with a power spectral analysis and a PPG morphological study to find out the best place to estimate the respiratory rate and its causes.

In this work, the PPG signal is recorded in the finger and forehead, and the PRV, PAV, PWV and RIIV signals are extracted from each location. The respiratory rate for these PDR signals (and all the possible combinations of them) is estimated and the success rate, the relative error and a confusion matrix are computed to evaluate how the location of the PPG sensor affects respiratory rate estimation. The power distribution of respiratory information and some morphological parameters of both PPG signals are also studied to complete the analysis. A preliminary version of this work was presented (Hernando *et al* 2017), where only the finger and forehead respiratory rate estimation from PAV was classified as correct or incorrect if matched with the reference, in a subset of ten subjects.

2. Materials

Thirty-five subjects (18 males and 17 females) with a mean age of 35.1 $\pm$ 6.5 years comprised the whole database. Throughout the test subjects remained comfortably seated for approximately half an hour. The protocol consisted of seven different stages with a duration of 3 min each: first, subjects were registered during spontaneous breathing; then a different respiratory rate was imposed in each of the remaining six stages, starting at 0.6 Hz and ending at 0.1 Hz in steps of 0.1 Hz. This controlled breathing is given by a sinusoidal wave that the subjects had to follow, marking the moment of inhale and exhale.

The finger and forehead PPG signals were recorded simultaneously as well as a chest-band respiratory signal. These signals were registered with the Medicom System, ABP-10 module (Medicom MTD, Ltd, Russia), a device specifically created to acquire raw biomedical signals without any pre-processing. The sample frequency was $f_s = 250$ Hz. Only the last 2 min of each stage are used to extract the features of the wave morphology and the respiratory information from the PPG signals. The results of the respiratory chest-band signal obtained the same respiratory rate imposed by the guided sinusoidal wave, so it was used as the reference to compare the respiratory rate estimated from the finger and forehead PPG.

3. Methods

3.1. PPG-derived respiration signals

First of all, a band-pass filter (cut-off frequencies of 0.3–35 Hz) was applied to both PPG signals ($x_{\mathrm{PPG}}(n)$) in order to avoid baseline noise and possible interferences (Garzón-Rey *et al* 2017). Then, artefactual pulses were suppressed by using the artefact detector described in Gil *et al* (2008). Finally, the apex ($n_{\mathrm{A}i}$), the basal ($n_{\mathrm{B}i}$) and the medium ($n_{\mathrm{M}i}$) points of the PPG pulses were automatically detected using an algorithm based on a low-pass differentiator filter (Lázaro *et al* 2014a). The medium points are considered to be the fiducial points in the PPG signal (Peralta *et al* 2019) in order to compute the pulse-to-pulse (PP_i) time series. The onset ($n_{\mathrm{O}i}$) and end ($n_{\mathrm{E}i}$) of the pulses were detected as described in Lázaro *et al* (2013). Figure 1 shows an example of the finger and forehead signals with their most representative points highlighted.

Finally, four PDR signals were obtained:

- Pulse rate variability (PRV) represents the time difference between two adjacent medium points (Bailón *et al* 2011):

$$d^{u}_{\mathrm{PRV}}(n) = \sum_{i} f_s \delta(n - n_{\mathrm{M}i})/(n_{\mathrm{M}i} - n_{\mathrm{M}i-1}). \quad (1)$$

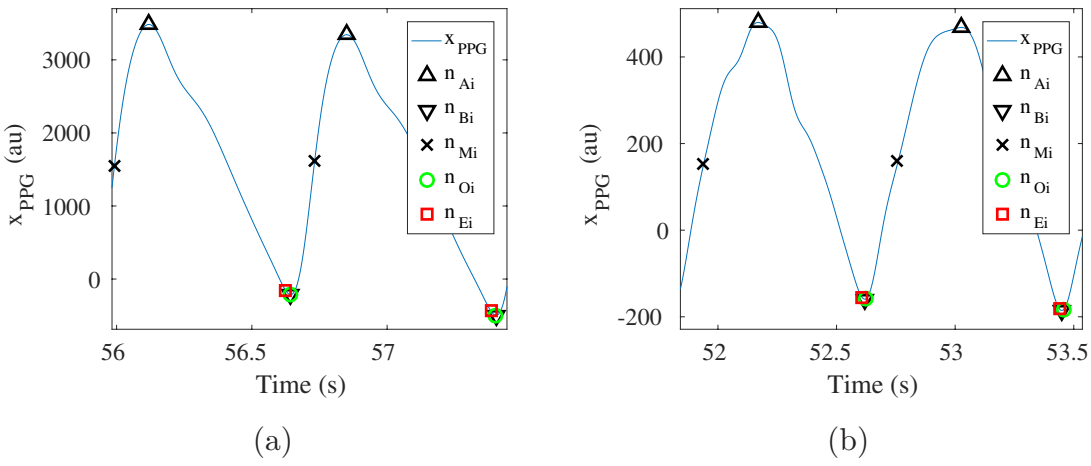

Figure 1. Two pulse waves of both PPG signals (left image, finger PPG; right image, forehead PPG; measured in arbitrary units, au) with their most representative points highlighted. Distance between the two adjacent medium points is the pulse-to-pulse interval or PP_i, used to compute the time series.

- Pulse amplitude variability (PAV) reflects the amplitude variation between the apex and the basal points (Lázaro *et al* 2013):

$$d^u_{\mathrm{PAV}}(n) = \sum_i \left[x_{\mathrm{PPG}}(n_{\mathrm{A}i}) - x_{\mathrm{PPG}}(n_{\mathrm{B}i})\right] \delta(n - n_{\mathrm{M}i}). \tag{2}$$

- Pulse width variability (PWV) reflects the width variation of the pulses:

$$d^u_{\mathrm{PWV}}(n) = \sum_i \frac{1}{f_s}(n_{\mathrm{E}i} - n_{\mathrm{O}i})\delta(n - n_{\mathrm{M}i}). \tag{3}$$

- Respiratory-induced intensity variability (RIIV) was estimated from the basal points (Karlen *et al* 2013). It must be noted that for this PDR signal the initial band-pass filter is not applied in order to maintain the intensity variations produced by respiration:

$$d^u_{\mathrm{RIIV}}(n) = \sum_i \left[x_{\mathrm{PPG}}(n_{\mathrm{B}i})\right] \delta(n - n_{\mathrm{M}i}). \tag{4}$$

The four PDR signals assume that their variations are due to a modulation based on respiratory information. These signals are unevenly sampled (superscript u) so a resampling at 4 Hz to standardize them is applied using cubic splines in addition to a median-absolute-deviation-based outlier rejection rule. Then, a band-pass filter (cut-off frequencies of 0.07–0.8 Hz) is applied over the PDR signals in order to limit the analysis to within the frequency range where the respiratory information is (Lázaro *et al* 2013). An example of the four PDR signals is shown in figure 2.

3.2. Respiratory rate estimation

A fusion technique based on a frequency analysis of the PDR signals (Lázaro *et al* 2013) is applied to estimate respiratory frequency ($\hat{F_{\mathrm{R}}}$) every 5 s from 'peaked-conditioned' averaged spectra. This method estimates a power spectrum density every 5 s from a 40 s length running window of each PDR signal using Welch's periodogram. The biggest peak near the previous respiratory rate estimation is selected, and the percentage of power around this peak with respect a reference interval is computed. If this percentage is higher than an established threshold (if the signal is peaked enough), it means that the respiratory information of this PDR signal is very clear, so this spectrum is promediated together with the other PDR spectra that were peaked enough, and a peaked-conditioned average spectra is obtained. The location of the largest peak in this average spectra is selected as the new respiratory rate estimation. This algorithm can be applied over a single PDR signal or over a combination of them, so results of the estimated respiratory rate using all the possible combination of PDR signals are considered.

The same method is applied over the respiratory chest-band information in order to obtain a reference of the real respiratory rate (F_{C}), which is going to be used as the reference to check every PDR signal and combination performance.

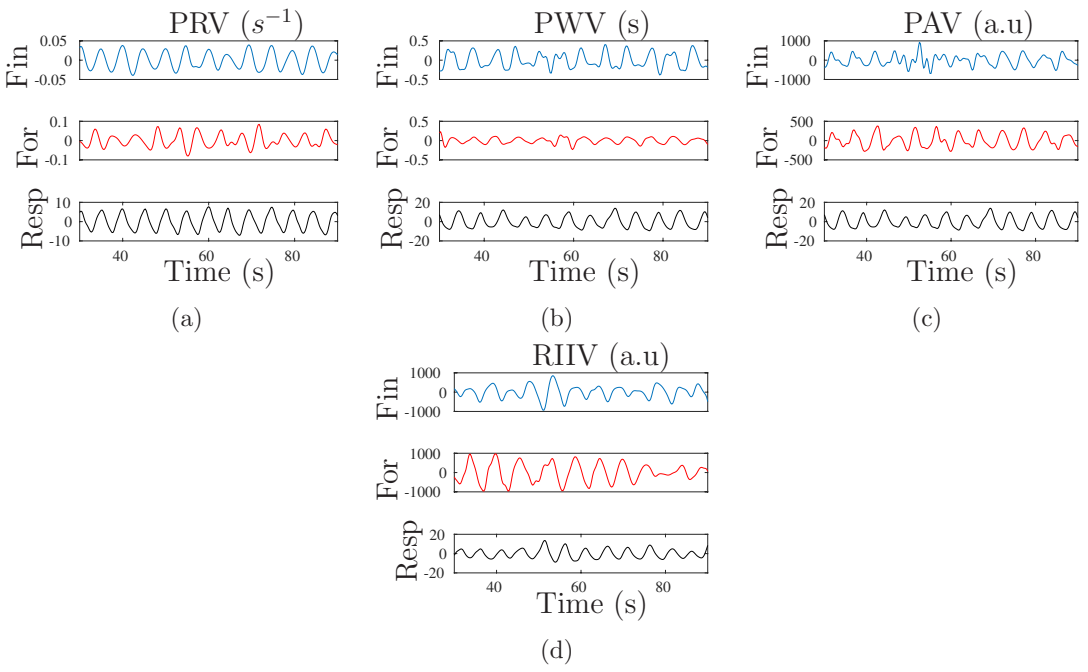

Figure 2. One-minute representation of the respiration extracted in the finger (Fin, in blue), in the forehead (For, in red) and the chest-band respiratory signal (Resp, in black) for the four PDR signals (PRV, PWV, PAV and RIIV).

3.3. Performance measurements and PDR signal characteristics

A comparison between the respiratory rate estimated with the PDR signals and from the reference is done every 5 s with an experimental margin of error of ±0.05 Hz (±0.3 bpm). If the estimation matches with the reference, it is considered as a correct estimation (CE), while an incorrect estimation (IE) is considered otherwise. The success rate is used as a performance measure:

$$\mathrm{SR} = \mathrm{CE}/(\mathrm{CE} + \mathrm{IE}) \times 100. \tag{5}$$

The inter-subject mean of this percentage is calculated for every stage and for each PDR signal and all possible combinations of them. Also, a confusion matrix was computed to analyse what happen when the respiratory rate was not successfully estimated.

In addition, the relative error (e_r) of the respiratory rate estimation is also calculated:

$$e_r = (\hat{F_R} - F_C)/F_C \times 100. \tag{6}$$

Another interesting point of study is the power distribution for each PDR signal. Thus, for each stage, the power within a bandwidth of 0.1 Hz around the expected respiratory frequency (given by the respiratory chest band, F_C) is compared with the total power in the spectra (from 0.07 to 0.65 Hz):

$$P_R(k) = \left(\int_{f=F_C-0.05}^{f=F_C+0.05} \bar{S}_k(f)\,df\right)/\left(\int_{f=0.07}^{f=0.65} \bar{S}_k(f)\,df\right), \tag{7}$$

where $\bar{S}_k(f)$ is the peaked-conditioned average spectra and k represents the time instant (every 5 s) (Lázaro *et al* 2013). This ratio aims to quantify how much power related to the respiratory component appears in each PDR signal in each stage, assuming than higher relative power means a greater respiratory signal-to-noise ratio.

The possible variations between each pair of PDR signals from the finger and the forehead could be due to differences in the wave morphology associated with the location (Allen 2007, Nilsson *et al* 2007). Therefore, the width and the pulse rate are analysed for each pulse of the PPG signal (denoted with the index *i*) in the finger and the forehead:

- Width: reflects the pulse width of each wave:

$$PW_i = n_{Ei} - n_{Oi}. \tag{8}$$

- Rate: reflects the difference between adjacent medium points:

$$PR_i = 1/(n_{Mi} - n_{Mi-1}). \tag{9}$$

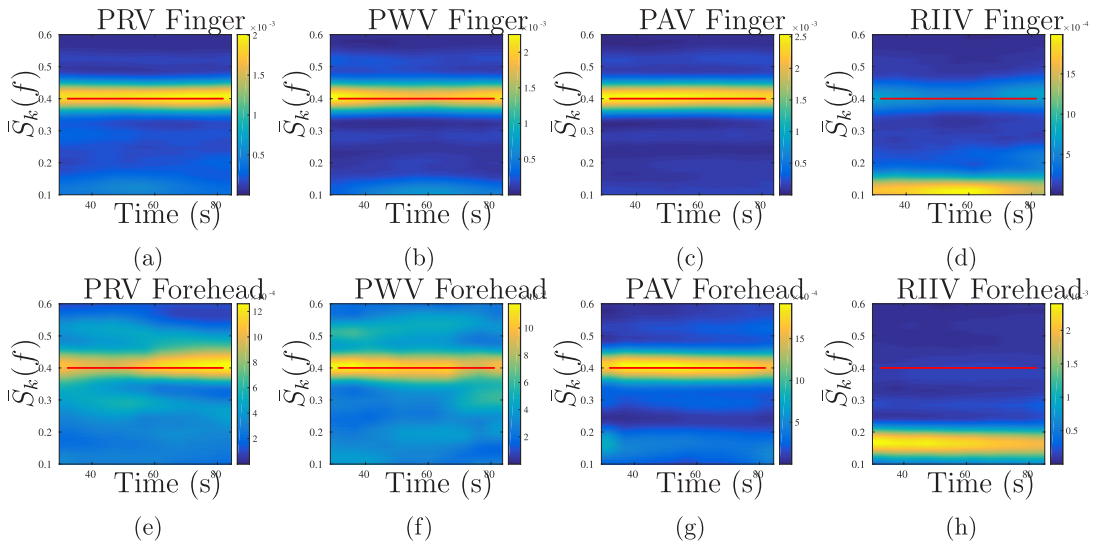

Figure 3. Time-frequency maps of the respiratory rate estimation using the finger (upper row) and the forehead (lower row) PPG signal with different PDR signals separately: (a) and (e) PRV; (b) and (f) PAV; (c) and (g) PWV; (d) and (h) RIIV. The red line represents the chest-band respiratory rate estimation.

Finally, statistical analysis is made to compare all these results obtained with the PPG signal registered in the finger and the forehead. First, a Shapiro–Wilk test is applied to verify the normal distribution of the data. The Student's t test is applied if the distribution is normal; otherwise, the Wilcoxon paired test is the one applied. In both methods, a p value of $\leqslant 0.05$ defines the significance.

4. Results

Figure 3 shows an example of the time-frequency maps ($\bar{S}_k(f)$) of eight different PDR signals during the controlled breathing stage at a respiratory rate of 0.4 Hz. Each row represents one different PPG signal (finger and forehead) and each column corresponds with one different PDR signal (PRV, PWV, PAV and RIIV). The image shows a high spectral power component (yellow zone) around the expected respiratory rate (red line) in six out of eight PDR signals. In the other two (RIIV extracted in the finger and forehead), the main frequency component is located between 0.1 and 0.2 Hz and is not related to respiration.

Table 1 shows the respiratory rate estimation success rate in each stage using a single PDR signal and with all the possible combinations of them, for both possible PPG sensor locations. The results show better performance of the algorithm at low respiratory rates and when the sensor is located in the finger. When only one PDR signal is used, PRV obtains the best results at lower frequencies, but when the frequency is above 0.2 Hz, PAV reaches the best results in the finger and PWV in the forehead. Good results are found when several signals are combined, especially with PRV–PWV, PWV–PAV and PRV–PWV–PAV. The worst results are found with the RIIV signal (and all its combinations) except at the 0.1 Hz stage. It must be noted that combining PDR signals does not imply an increase in success rate.

Table 2 shows the relative error of each single PDR signal and with all the possible combinations of them for both possible PPG sensor locations. It must be noted that the error is usually negative (except at the 0.1 Hz stage). This indicates that the estimated respiratory rate is lower than the real respiratory rate. The results show a lower error when the sensor is located in the finger and when the respiratory rate is low. Similar to table 1, the lower error is found in PAV in the finger and in PWV in the forehead when only one PDR signal is used. Also, combinations that show a low error are PWV–PAV and PRV–PWV–PAV.

Due to the differences found in the respiratory rate estimation of every PDR signal, a study of the four PDR signals separately is done to analyse the causes of the differences between the locations of the PPG sensor. Table 3 shows four confusion matrices where all the estimations of each single PDR signal are compared with respect to the reference respiratory rate given by the chest band for both possible PPG sensor locations. The results show higher accuracy at lower frequencies and in finger estimations with respect to forehead estimations. In PRV, PWV and PAV the diagonal presents the highest values (this indicates than the estimation matches with the reference) except at the 0.6 Hz stage in PRV and PAV. In RIIV, in all the stages except at 0.2 Hz, the highest percentage of estimations is found in the 0.1 Hz stage in the finger and in 0.1 and 0.2 Hz stages in the forehead. This means that, when an error occurs, the respiratory rate estimation is 0.1 or 0.2 Hz in most of the cases. This result is in agreement with the poor success rate showed in table 1 and with the large negative error in table 2.

Table 1. Mean ± std of the respiratory rate estimation success rate (*SR*) using the PDR signals separately and all the possible combinations of them, in both locations (Fin for the finger and For for the forehead). The best results of each stage (single, double or triple combination) are highlighted in bold. Significant differences between the finger and forehead values are indicated with ∗ ($p < 0.01$) or with ∗∗ ($p < 0.001$).

—	Zone	PRV	PWV	PAV	RIIV	PRV PWV	PRV PAV	PRV RIIV	PWV PAV	PWV RIIV	PAV RIIV	PRV PWV PAV	PRV PWV RIIV	PRV PAV RIIV	PWV PAV RIIV	PRV PWV PAV RIIV
Spt	Fin	70.4±	69.0±	**77.1**±	31.2±	**76.8**±	68.3±	37.4±	68.8±	36.6±	36.1±	**66.7**±	37.9±	37.4±	36.6±	37.4±
		38.5	40.7	**40.3**	43.5	**36.9**	40.3	43.1	39.7	42.7	42.9	**40.9**	43.5	43.6	42.9	43.6
	For	51.5±	58.4±	**63.4**±	33.8±	57.5±	60.9±	37.2±	**72.5**±	43.7±	40.1±	**59.0**±	38.5±	39.0±	45.0±	39.2±
		46.3∗	41.8	**39.3**	42.6	45.7∗	43.0	46.5	**36.7**	43.4	42.8	**44.7**	46.2	46.5	43.3	46.0
0.1	Fin	**97.4**±	79.9±	85.5±	94.6±	**97.4**±	**97.4**±	**97.4**±	91.9±	94.0±	**97.4**±	**97.4**±	**97.4**±	**97.4**±	**97.4**±	97.4±
		15.2	34.4	33.5	22.4	**15.2**	**15.2**	**15.2**	24.6	22.5	**15.2**	**15.2**	**15.2**	**15.2**	**15.2**	15.2
	For	**97.1**±	76.2±	43.6±	78.7±	94.5±	**97.1**±	95.3±	65.2±	86.8±	78.4±	**97.1**±	95.6±	95.3±	87.6±	95.6±
		14.1	38.6	43.4∗∗	38.8	20.5	**14.1**	17.4	42.0∗	26.3	38.9∗	**14.1**	16.5	17.4	26.7∗	16.5
0.2	Fin	**91.0**±	90.0±	86.3±	56.5±	89.0±	90.0±	64.7±	**91.1**±	57.5±	57.1±	**87.4**±	63.8±	62.3±	56.0±	61.4±
		25.9	26.2	30.9	45.0	28.1	26.9	44.6	**24.4**	44.7	46.5	**30.0**	43.8	45.2	45.9	44.5
	For	**77.3**±	76.6±	54.9±	59.8±	**80.1**±	69.1±	59.2±	70.1±	65.2±	59.3±	**75.1**±	56.0±	58.9±	64.3±	56.0±
		32.8	35.1	44.4∗	44.4	**31.8**	38.5∗	44.9	39.8∗	41.6	43.4	**36.0**	45.7	44.6	43.0	45.7
0.3	Fin	83.1±	77.7±	**89.3**±	30.6±	81.8±	82.1±	43.5±	**86.8**±	39.7±	38.2±	**80.0**±	46.3±	44.9±	41.3±	45.4
		34.2	38.0	**24.7**	44.1	37.1	35.5	45.8	**31.4**	45.0	47.1	**37.4**	45.3	46.1	45.9	45.9
	For	58.0±	**72.4**±	63.3±	2.9±	64.5±	63.7±	10.1±	**73.4**±	12.4±	15.4±	**63.6**±	12.6±	15.7±	18.6±	16.2±
		45.0∗∗	**39.5**	46.7∗	16.9∗∗	42.1∗	41.0	24.5∗∗	**37.9**	29.3∗∗	30.8∗	**41.7**	27.5∗∗	28.7∗∗	33.3∗	30.7∗∗
0.4	Fin	68.3±	58.7±	**78.6**±	30.4±	58.4±	**66.0**±	35.9±	61.2±	26.0±	39.0±	**57.4**±	29.1±	38.3±	28.6±	28.6±
		45.8	46.9	**39.4**	45.9	48.2	**46.4**	45.2	43.8	43.3	44.5	**47.3**	44.0	44.0	42.4	42.4
	For	45.1±	**60.0**±	55.1±	1.3±	**54.0**±	44.9±	2.6±	51.6±	8.3±	5.3±	**44.6**±	4.7±	4.2±	9.6±	5.7±
		47.4	**42.7**	43.6∗	7.7∗∗	**46.9**	46.1∗	13.9∗∗	44.3	23.8∗	17.2∗∗	**46.0**	17.4∗	15.2∗∗	23.4∗	18.2∗
0.5	Fin	57.7±	51.1±	**75.8**±	17.4±	53.9±	57.4±	17.4±	**61.3**±	17.9±	21.8±	**55.8**±	17.7±	20.3±	22.1±	20.0±
		49.6	47.3	**40.7**	36.5	48.8	49.1	36.5	**45.1**	36.9	38.8	**47.6**	36.8	38.5	39.5	38.6
	For	40.0±	**45.2**±	40.3±	0.0±	37.4±	**40.2**±	2.9±	37.8±	0.0±	3.9±	**33.7**±	1.8±	2.9±	1.6±	1.8±
		41.3	**46.5**	47.2∗	0.0∗	44.2	**43.7**	16.9∗	46.1∗	0.0∗	16.4∗	**42.3**	10.7∗	16.9∗	9.2∗	10.8∗
0.6	Fin	36.4±	45.4±	**46.5**±	10.1±	32.2±	34.0±	8.6±	**43.4**±	8.6±	8.6±	**34.0**±	8.6±	8.6±	8.6±	8.6±
		47.2	48.7	**48.0**	29.4	45.9	46.3	28.4	**46.2**	28.4	28.4	**46.3**	28.4	28.4	28.4	28.4
	For	27.8±	**33.5**±	20.5±	0.0±	**26.5**±	15.3±	0.8±	14.5±	0.8±	1.8±	**17.9**±	0.0±	0.8±	1.6±	0.5±
		41.4	**45.3**	37.0∗	0.0	**42.7**	31.3	3.4	32.0∗∗	4.6	8.2	**33.5**	0.0	3.4	6.8	3.1

Figure 4 shows the boxplots of the relative power ($\overline{P_R}$) in normalized units (n.u.). $\overline{P_R}$ in the finger is higher than in the forehead and it decreases when the frequency increases in the four PDR signals. PWV is the one that shows the least significant differences in both locations, only at the 0.2 and 0.3 Hz stages.

We found not only differences in the power distribution; we also noted morphological differences between the two PPG signals extracted in the finger and the forehead. Figure 5 shows the width and rate of the PPG signal at both locations. The width is higher in the forehead than in the finger but the rate remains nearly equal for both signals.

5. Discussion

In this paper, an evaluation of how the location of the PPG sensor affects the respiratory rate estimation and which PDR signals are more appropriate for this purpose has been performed. PPG signals were recorded in the finger and forehead from subjects breathing spontaneously and at different controlled respiratory rates. A four-PDR technique was applied to both locations of the PPG signals, obtaining one respiratory rate estimation per PDR signal. In addition, the respiratory rate was also estimated from all the possible combinations of these four PDR signals. The estimations were compared with the respiratory rate estimated from the chest band, which was taken as reference. A respiratory estimation was considered to be accurate if it differed less than 0.05 Hz (0.3 bpm) from the reference, based on the errors reported in the PDR methods (Lázaro *et al* 2013). The success rate and the relative error of the estimated respiratory rate from both locations are presented, as well as a confusion matrix for each PDR signal, to evaluate their performance. Also, the power distribution of the respiratory information and

Table 2. Mean ± std of the percentage of the relative error (e_r) committed in the respiratory rate estimation by each PDR signal separately and with all the possible combinations of them, in both locations (Fin for the finger and For for the forehead). The best results of each stage (single, double or triple combination) are highlighted in bold. Significant differences between the finger and forehead values are indicated with an ∗ ($p < 0.01$) or with a ∗∗ ($p < 0.001$).

—	Zone	PRV	PWV	PAV	RIIV	PRV PWV	PRV PAV	PRV RIIV	PWV PAV	PWV RIIV	PAV RIIV	PRV PWV PAV	PRV PWV RIIV	PRV PAV RIIV	PWV PAV RIIV	PRV PWV PAV RIIV
Spt	Fin	−17.3± 22.3	**−8.2± 27.9**	−9.3± 19.1	−40.4± 23.7	**−14.7± 22.3**	−17.5± 22.2	−36.8± 23.5	−15.2± 21.2	−36.7± 23.6	−37.4± 23.3	**−17.6± 22.6**	−36.5± 23.7	−36.7± 23.7	−37.2± 23.3	−36.7± 23.7
	For	−21.8± 34.0	**1.9± 43.3**	17.0± 41.4	−29.3± 24.1∗∗	−23.5± 23.7	−20.0± 23.7	−33.6± 23.0	**2.7± 34.9∗**	−24.4± 23.0∗	−22.7± 28.7∗∗	**−20.3± 25.2**	−32.6± 22.3	−32.7± 22.0	−24.6± 21.9∗∗	−32.4± 22.1
0.1	Fin	**−1.1± 7.7**	14.8± 30.1	11.3± 33.6	1.3± 16.8	**−1.1± 7.7**	−1.3± 7.6	−1.9± 7.5	3.3± 18.9	1.6± 16.9	−1.5± 7.7	**−1.4± 7.6**	−1.9± 7.5	−1.9± 7.5	−1.5± 7.7	−2.0± 7.5
	For	**0.4± 8.8**	34.8± 72.3∗	94.4± 95.7∗∗	19.2± 27.1∗∗	2.3± 14.7	**0.9± 9.3**	1.6± 11.3	56.5± 87.3∗∗	8.4± 18.1∗	19.2± 27.3∗∗	**0.8± 9.3**	1.4± 11.0	1.6± 11.3	8.4± 19.0∗∗	1.4± 11.0
0.2	Fin	−4.3± 11.6	−4.6± 10.8	**−1.6± 15.4**	−20.4± 20.6	−5.5± 12.9	−4.9± 12.4	−16.9± 20.6	**−4.5± 11.4**	−20.1± 20.4	−20.2± 21.3	**−6.4± 13.9**	−17.4± 20.3	−18.0± 21.0	−20.8± 20.9	−18.5± 20.6
	For	**−4.2± 22.6**	6.3± 19.8∗	31.4± 50.4∗∗	−19.6± 16.0	−7.4± 15.5	**2.2± 33.4**	−20.4± 15.5	16.2± 32.2∗	−13.8± 18.6	−12.7± 24.4	**−4.2± 23.4**	−17.9± 22.9	−20.2± 15.7	−12.9± 22.7	−17.9± 22.9
0.3	Fin	−9.8± 20.9	−10.5± 20.7	**−5.5± 14.3**	−42.6± 28.4	−10.9± 22.5	−10.3± 21.3	−34.4± 28.7	**−7.6± 18.4**	−36.7± 28.4	−38.2± 29.6	**−11.8± 22.3**	−32.7± 28.6	−33.7± 29.2	−35.9± 28.7	−33.4± 29.0
	For	−18.3± 28.6	**−7.3± 21.3**	−10.8± 25.5	−49.1± 11.2	−14.3± 28.2	−18.6± 23.0	−46.7± 16.5∗	**−12.6± 20.2**	−44.6± 17.0	−41.7± 18.0	**−19.5± 23.7**	−46.5± 16.3∗	−44.5± 17.3	−41.0± 18.9	−44.7± 18.4
0.4	Fin	−22.6± 32.7	−24.1± 28.7	**−15.4± 28.2**	−50.2± 33.5	−27.9± 33.3	**−24.2± 33.5**	−45.2± 32.8	−24.9± 30.1	−51.4± 31.4	−43.0± 32.8	**−29.2± 33.7**	−49.4± 31.8	−43.7± 32.5	−49.8± 31.0	−49.7± 30.9
	For	−34.6± 32.1	**−17.3± 20.7**	−22.3± 27.4	−62.7± 7.3	−28.6± 30.7	−32.2± 28.9	−61.5± 10.5∗	**−24.4± 25.7**	−57.3± 15.7	−58.7± 14.0∗	**−32.4± 28.3**	−60.4± 12.4	−60.4± 11.6∗	−56.1± 16.7	−59.5± 13.3
0.5	Fin	−30.6± 37.1	−29.9± 31.7	**−16.4± 29.5**	63.9± 28.7	−34.1± 37.1	−31.3± 37.0	−64.0± 28.6	**−25.0± 31.1**	−61.9± 29.4	−59.7± 30.8	**−31.5± 35.5**	−63.4± 28.8	−61.4± 30.3	−58.8± 31.0	−61.5± 30.3
	For	−35.5± 31.5	**−30.7± 29.8**	−31.0± 27.5∗	−70.3± 4.4	−37.3± 31.8	−35.3± 30.3	−69.1± 12.8	**−34.4± 29.4**	−69.7± 5.2	−65.6± 14.0	**−39.1± 29.6**	−68.9± 9.5	−67.9± 13.1	−67.7± 10.1	−68.5± 9.7
0.6	Fin	−44.3± 36.1	−36.6± 34.8	**−28.6± 31.7**	−70.7± 25.8	−51.1± 37.3	−43.9± 35.7	−72.4± 23.7	**−37.4± 34.7**	−71.8± 24.0	−72.1± 23.9	**−49.6± 37.2**	−72.8± 23.6	−72.3± 23.8	−72.5± 23.8	−72.5± 23.9
	For	−45.1± 33.5	**−40.1± 31.9**	−45.7± 28.5∗	−75.2± 4.1	**−47.9± 33.0**	−55.0± 26.6	−74.0± 8.9	−54.4± 25.8∗	−73.7± 9.6	−72.4± 9.9	**−54.9± 27.7**	−74.3± 7.9	−72.6± 12.2	−72.3± 11.0	−74.1± 8.2

Table 3. Confusion matrix of each PDR signal comparing each respiratory rate estimation (vertical axis) with the reference given by the chest band (horizontal axis), in both locations (Fin for the finger and For for the forehead). The best results of each stage are highlighted in bold.

PRV	Zone	Spt	0.1	0.2	0.3	0.4	0.5	0.6
Spt	Fin	**267**	0	0	0	0	0	0
	For	**196**	0	0	0	0	0	0
0.1	Fin	91	**371**	34	55	119	144	**177**
	For	152	**377**	65	114	150	125	**147**
0.2	Fin	18	0	**348**	8	0	5	11
	For	12	2	**292**	19	18	24	32
0.3	Fin	1	0	0	**317**	2	4	16
	For	1	0	9	**220**	30	22	13
0.4	Fin	2	0	0	0	**259**	8	11
	For	14	0	9	24	**174**	49	39
0.5	Fin	0	0	0	0	0	**220**	26
	For	2	0	1	3	0	**152**	39
0.6	Fin	0	0	0	0	0	0	140
	For	0	0	0	0	0	2	107

PWV	Zone	Spt	0.1	0.2	0.3	0.4	0.5	0.6
Spt	Fin	**262**	0	0	0	0	0	0
	For	**221**	0	0	0	0	0	0
0.1	Fin	75	**305**	34	48	90	88	98
	For	55	**301**	27	41	44	72	101
0.2	Fin	17	66	**346**	30	34	45	56
	For	45	32	**289**	40	18	41	51
0.3	Fin	21	0	2	**298**	30	36	20
	For	38	36	42	**276**	86	63	35
0.4	Fin	4	0	0	4	**226**	18	29
	For	2	6	18	21	**224**	26	23
0.5	Fin	0	0	0	0	0	**194**	3
	For	5	4	0	2	0	**172**	38
0.6	Fin	0	0	0	0	0	0	**175**
	For	11	0	0	0	0	0	**129**

PAV	Zone	Spt	0.1	0.2	0.3	0.4	0.5	0.6
Spt	Fin	**291**	0	0	0	0	0	0
	For	**243**	0	0	0	0	0	0
0.1	Fin	84	**326**	40	30	79	74	92
	For	5	**169**	19	45	65	34	63
0.2	Fin	0	38	**330**	11	0	0	7
	For	35	89	**208**	64	64	100	**119**
0.3	Fin	2	7	2	**339**	3	0	24
	For	26	41	42	**240**	22	47	30
0.4	Fin	2	0	10	0	**298**	17	18
	For	60	76	83	27	**214**	45	48
0.5	Fin	0	0	0	0	0	**290**	60
	For	6	4	22	4	7	**148**	39
0.6	Fin	0	0	0	0	0	0	**180**
	For	2	0	2	0	0	0	78

RIIV	Zone	Spt	0.1	0.2	0.3	0.4	0.5	0.6
Spt	Fin	117	0	0	0	0	0	0
	For	130	0	0	0	0	0	0
0.1	Fin	**255**	**361**	166	**254**	**264**	**310**	**320**
	For	**162**	**298**	145	**198**	**203**	**192**	**203**
0.2	Fin	17	10	**216**	10	1	2	0
	For	79	81	**229**	171	163	182	172
0.3	Fin	0	0	0	116	1	0	13
	For	6	0	0	11	1	0	1
0.4	Fin	0	0	0	0	114	2	7
	For	0	0	2	0	5	0	0
0.5	Fin	0	0	0	0	0	67	1
	For	0	0	0	0	0	0	1
0.6	Fin	0	0	0	0	0	0	40
	For	0	0	0	0	0	0	0

the rate and the width of each different PPG signal are analysed in order to try to explain the differences between the sensor locations.

Focusing on the finger and forehead, since they are the most extended locations of PPG sensor, it can be seen that a change in the place where the PPG signal is registered involves other variations that should be considered: different locations imply different configurations in signal acquisition (Allen 2007), as a light-transmission configuration can be used in the finger but not in the forehead, where light reflection is the only possible configuration; the optical features of the skin are not the same in the finger than in the forehead; also the peripheral blood flow varies from one location to another because different capillary vessels irrigate the different zones. These changes affect the PPG morphology, obtaining a smoother waveform when the signal is recorded in the forehead than in the finger (Allen 2007, Nilsson *et al* 2007). Our hypothesis supposes that this change in the waveform may affect PDR signals, with a decrease in the modulation that respiration induces over these signals. As the same PDR signal is different depending on the PPG sensor location, respiratory rate estimation could be affected by this variable. In fact, an important conclusion of this study is that respiratory rate estimation is more accurate when the PPG signal is recorded in the finger than in the forehead, as other studies pointed out (Charlton *et al* 2017). The success rate is higher and the relative error is lower in the finger than in the forehead for all stages and all PDR signals. In addition, the diagonal of the confusion matrix shows a higher number of correct estimations in the finger than in the forehead.

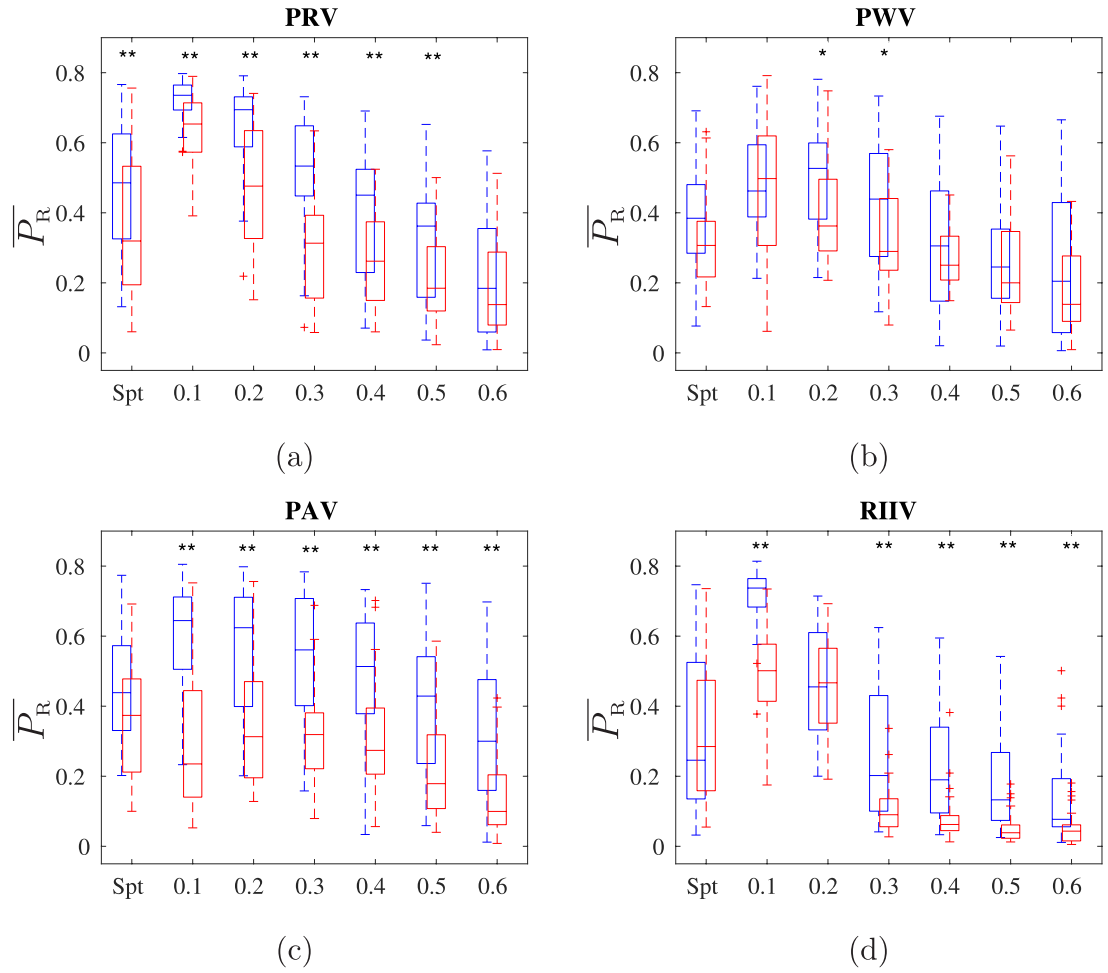

Figure 4. Boxplots of $\overline{P_R}$ from finger (blue) and forehead (red) PPG using a single PDR signal: (a) PRV; (b) PWV; (c) PAV; (d) RIIV. Significant differences between the finger and forehead values are indicated with an $*$ ($p < 0.01$) or with a $**$ ($p < 0.001$).

One possible explanation of this better results in the finger lies in the relative power of the respiratory band normalized to the entire spectra, represented in figure 4, where recordings in the finger show a higher $\overline{P_R}$ than in the forehead. A higher $\overline{P_R}$ means that the respiratory component can be more easily identified, and therefore, the respiratory rate estimator has a greater chance to give a correct result. On the other hand, with a lower value of $\overline{P_R}$, it is easier to misunderstand the respiratory component and consequently getting an incorrect estimation. The power around the respiratory component was also studied in Nilsson *et al* (2007), where the frequency component analysis shows the lower power in the finger compared to other sensor locations. However, our results show the opposite (see figure 4), indicating a minor respiratory-related component in the forehead mainly at high frequency rates. It is worth noting some differences between Nilsson's work and our work: in his study, signals were recorded in the supine position where parasympathetic activity is enhanced, and the methodology used was based on the analysis of the PPG signal spectrum (Nilsson *et al* 2007), while our recordings are in sitting position and the analysed spectral power is extracted from the PDR signals. Therefore the counterbalance of respiratory-related and respiratory-unrelated components of the PDR signals seems to be essential, at least for frequency-based methods.

Concerning which PDR signal is the best to estimate the respiratory rate, PRV showed the best results for lower frequencies (below 0.3 Hz), with a higher success rate, a lower relative error and a higher number of correct estimations. However, its performance is not so good for higher frequencies. Above 0.3 Hz, PAV was the one with the best results when PPG is registered in the finger, although the results at lower frequencies are quite acceptable, too. However, PAV shows not so good results in the forehead; in fact significant differences have been found in the success rate and the power around the respiratory component between the locations. These bad results of PAV in the forehead were noted in our preliminary study (Hernando *et al* 2017), but in that work the preliminary filter used to remove the baseline noise was not applied and the results obtained were worse. As another work suggests (Sun *et al* 2019), removing the baseline modulation increases the success rate of the PAV signal in the forehead (if not, the results were as bad as the RIIV forehead ones), although its performance is not as good as in the finger. On the other hand, PWV has the best results in the forehead, especially in frequencies above 0.3 Hz. PWV is the only PDR signal whose results in the finger are quite similar to the forehead ones. This could be explained by the simi-

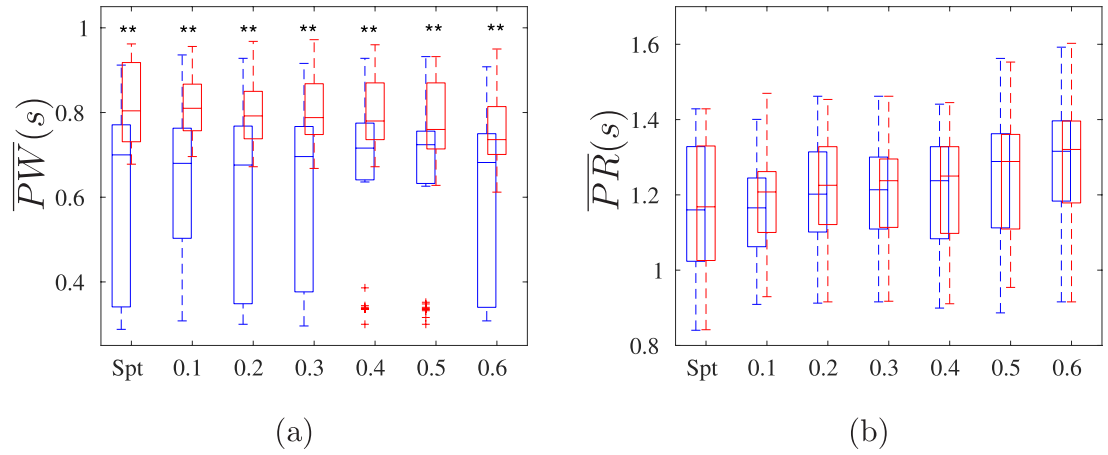

Figure 5. Boxplots of the morphological parameters extracted from the finger (blue) and forehead (red) PPG signals. Significant differences between the finger and forehead values are indicated with an $*$ ($p < 0.01$) or with a $**$ ($p < 0.001$).

lar distribution of the power related to the respiratory component in both locations (see figure 4), with almost no differences between the sites. The good performance of PRV, PWV and PAV were noted in Dash *et al* (2010) and Lázaro *et al* (2013). RIIV, although a very common PDR signal used in many studies (Nilsson *et al* 2000, Karlen *et al* 2013, Lin *et al* 2013), obtained the worst results. However, it must be highlighted that in these studies subjects were breathing spontaneously and none of them had studied RIIV signal registered in the forehead. The worst result with RIIV could be explained by the spectral component, which was not related to respiration. It must be noted that these four PDR signals have been studied in this specific database, which is comprised of healthy subjects with a mean age of 35.1 ± 6.5 years. However, in the study of a different database with different subjects, maybe some of these PDR signals could be eliminated as they could not provide faithful respiratory information. For example, while in this database PAV seems to be the one with the best performance, in a different database comprised of patients with a fluid overload, PAV may not provide valid information (Javed *et al* 2010). Otherwise, in an elderly database, where respiratory sinus arrhythmia would not be so significant (De Meersman 1993), PRV performance should decrease. Therefore, the inclusion of each PDR signal in the respiratory rate estimation method should be considered depending on the final application. Finally, the combination of PDR signals does not give the method more robustness; moreover, results with a combination of PDR signals are worse in the higher frequency stages. This result is in contrast with the conclusion extracted from several works (Karlen *et al* 2013, Lázaro *et al* 2013), where the PDR signal combination offers more accurate estimations.

Another important conclusion of this work is the best performance of the respiratory estimation at lower frequencies than at higher ones. As table 1 shows, the success rate decreases 30% from 0.2 to 0.5 Hz stages in almost all the PDR signals (except in PAV) and for both body locations. Consequently, the error committed is higher in 0.5 Hz stage (more than a 25% with respect the 0.2 Hz stage). The spontaneous respiratory stage also shows good results because the respiratory rate during rest usually is in the lower frequency range, with a mean value of 0.23 Hz in this database. The relative error in spontaneous breathing is slightly higher than in 0.3 Hz stage because six subjects have a respiratory rate above 0.3 Hz, as it is more difficult to properly estimate respiratory rate in these cases. The best performance of the respiratory estimation at lower frequencies than at higher ones has also been reported in other studies (Johnston and Mendelson 2004, Addison *et al* 2015, Charlton *et al* 2017). Figure 4 shows less respiratory relative power as the respiratory rate increases for the four PDR signals. The respiratory rate is the only difference in the setup of the different stages, so we interpret that the lower relative power is due to less powerful respiration-related modulation. In the case of PRV, this is coherent with the well-known decrease of respiratory sinus arrhythmia as respiratory rate increases (Hirsch and Bishop 1981). A possible reason for this observation is that the autonomic nervous system may act as a physiological low-pass filter. That would explain also the effect in PAV and PWV. However, PRV and PWV are affected also by the mechanical effect of respiration on intrathoracic blood pressure, which may also show low-pass behaviour (Lázaro *et al* 2014b).

The decrease of the power of the respiratory spectral component at high breathing rates causes that other spectral components non-related with respiration become relevant and act as a confounding factor. Our results suggest the presence of a non-respiratory-related spectral component around 0.1 and 0.2 Hz (see figure 3, especially in RIIV). When an error occurs, respiratory rate estimation based on PDR is usually around 0.15 Hz. In fact, in table 3 the higher values of the confusion matrix are found either at the expected stage or at 0.1–0.2 Hz. This component, probably related to Mayer waves, and the problems that may cause for respiratory rate estimation have been pointed out in others works (Karlen *et al* 2013), and could significantly influence the PPG signal in the forehead (Pfurtscheller *et al* 2018). If the respiratory rate of one specific application is expected to be higher

than 0.15 Hz, a more restrictive filter with a higher value of the low cut-off frequency could be applied to try to overcome this non-respiratory-related component. In this work, a trial with 0.15 Hz as the low cut-off frequency of the filter that isolates the respiratory components has been implemented, and the results show an increase of greater than 20% in the success rate for all the single PDR signals when the PPG is registered in the finger and an increase of 10% in the forehead.

An analysis of the morphology of the PPG waveform is also presented in order to study how different the finger and forehead waves are, and whether PPG morphology is affected by the respiratory rate or not. The results show a greater width when the PPG is registered in the forehead in comparison with the finger, independently of the respiratory rate. These differences imply morphological changes between the locations, as other studies in the bibliography shown (Allen 2007, Nilsson *et al* 2007). However, the results do not show that these morphological changes cause restrictions in respiratory rate estimation. In the case of the width of the pulses, a greater width does not imply a decrease in the modulation that the respiration induces over the PWV signal. Therefore, respiratory rate estimation is apparently more affected by the ratio between the respiratory power with respect to the entire spectra that could mask the respiratory information than by morphological factors.

6. Conclusion

It has been shown that differences in the respiratory rate estimation and changes in morphological features are found when the PPG signal is recorded in the finger and in the forehead. The general results for respiratory rate estimation are characterized by better performance in the low frequencies and when the sensor is located in the finger when compared to the forehead. Also, RIIV showed poor performance, and when RIIV was combined with other PDR signals it negatively affected the accuracy of the estimation. Therefore, the finger is the recommended location for PPG signal acquisition, and the RIIV signal is not recommended, especially when the respiratory rate could increase to higher values. For this specific database, although PRV in the finger obtained good results at lower frequencies, the use of PAV in the finger would be preferable because it also obtains good results at lower frequencies (above 85% success rate at 0.1 and 0.2 Hz) and the best results at higher frequencies (almost 90% success rate at 0.3 Hz and above 75% at 0.4 and 0.5 Hz) and during spontaneous breathing (almost 80% success rate). The inclusion of each PDR signal in the fusion algorithm should be analysed for each specific application considering both the subject population and the breathing pattern, taking into account the effect of these factors on the respiratory modulation of the PPG.

Acknowledgments

This work has been partially financed by Ministerio de Economía, Industria y Competitividad (MINECO), and by fondos FEDER through Project Nos. PGC2018-095936-B-I00 and RTI2018-097723-B-I00, and by Centro Universitario de la Defensa (CUD) under Project Nos. CUD2018-08 and UZCUD2017-TEC-04. This work would not have been possible without collaboration from all volunteers (special mention to the CUD faculty) and the support of Gobierno de Aragón (Reference Group BSICoS T39-17R) co-funded by FEDER 2014–2020. This project has received funding from the European Union's Framework Programme for Research and Innovation Horizon 2020 (2014–2020) under the Marie Skłodowska-Curie Grant Agreement No. 745755. The computation was performed by the ICTS NANBIOSIS, specifically by the High Performance Computing Unit of CIBER-BBN at the University of Zaragoza.

ORCID iDs

A Hernando https://orcid.org/0000-0003-2596-7237
M D Peláez-Coca https://orcid.org/0000-0002-0690-3193
M T Lozano https://orcid.org/0000-0003-0630-4366
J Lázaro https://orcid.org/0000-0001-8742-0072
E Gil https://orcid.org/0000-0001-7285-0715

References

Addison P S, Watson J N, Mestek M L, Ochs J P, Uribe A A and Bergese S D 2015 Pulse oximetry-derived respiratory rate in general care floor patients *J. Clin. Monit. Comput.* **29** 113–20

Allen J 2007 Photoplethysmography and its application in clinical physiological measurement *Physiol. Meas.* **28** R1–39

Bailón R, Laouini G, Grao C, Orini M, Laguna P and Meste O 2011 The integral pulse frequency modulation with time-varying threshold: application to heart rate variability analysis during exercise stress testing *IEEE Trans. Biomed. Eng.* **58** 642–52

Challoner A V J and Ramsay C A A Photoelectric plethysmograph for the measurement of cutaneous blood flow *Phys. Med. Biol.* **19** 317–28 (https://iopscience.iop.org/article/10.1088/0031-9155/19/3/003/pdf)

Charlton P H, Bonnici T, Tarassenko L, Alastruey J, Clifton D A, Beale R and Watkinson P J 2017 Extraction of respiratory signals from the electrocardiogram and photoplethysmogram: technical and physiological determinants *Physiol. Meas.* **38** 669–90

Chon K H, Dash S and Ju K 2009 Estimation of respiratory rate from photoplethysmogram data using time-frequency spectral estimation *IEEE Trans. Biomed. Eng.* **56** 2054–63

Dash S, Shelley K H, Silverman D G and Chon K H 2010 Estimation of respiratory rate from ECG, photoplethysmogram, and piezo-electric pulse transducer signals: a comparative study of time frequency methods *IEEE Trans. Biomed. Eng.* **57** 1099–107

De Meersman R E 1993 Aging as a modulator of respiratory sinus arrhythmia *J. Gerontol.* **48** B74–8

Garzón-Rey J M, Lázaro J, Milagro J, Gil E, Aguiló J and Bailón R 2017 Respiration-guided analysis of pulse and heart rate variabilities for acute emotional stress assessment *Proc. XLIV Int. Conf. Computing in Cardiology* pp 1–4 (https://ieeexplore.ieee.org/stamp/stamp.jsp?arnumber=8331714)

Gil E, Orini M, Bailón R, Vergara J M, Mainardi L and Laguna P 2010 Photoplethysmography pulse rate variability as a surrogate measurement of heart rate variability during non-stationary conditions *Physiol. Meas.* **31** 1271–90

Gil E, Vergara J M and Laguna P 2008 Detection of decreases in the amplitude fluctuation of pulse photoplethysmography signal as indication of obstructive sleep apnea syndrome in children *Biomed. Signal Process. Control* **3** 267–77

Hartmann V, Liu H, Chen F, Qiu Q, Hughes S and Zhenq D 2019 Quantitative comparison of photoplethysmographic waveform characteristics: effect of measurement site *Front. Physiol.* **10** 198–205

Hernando A, Peláez-Coca M D, Lozano M T, Aiger M, Gil E and Lázaro J 2017 Finger and forehead PPG signal comparison for respiratory rate estimation based on pulse amplitude variability *25th European Signal Processing Conf. (EUSIPCO)* Kos (Greece) pp 2076–80 (https://ieeexplore.ieee.org/abstract/document/8081575)

Hertzman A B and Spielman C 1937 Observations on the finger volume pulse recorded photoelectrically *Am. J. Physiol.* **119** 334–5 (http://www.oalib.com/references/13686191)

Hirsch J A and Bishop B 1981 Respiratory sinus arrhythmia in humans: how breathing pattern modulates heart rate *Am. J. Physiol.* **241** H620–9

Javed F, Middleton P M, Malouf P, Chan G S H, Savkin A V, Lovell N H, Steel E and Mackie J 2010 Frequency spectrum analysis of finger photoplethysmographic waveform variability during haemodialysis *Physiol. Meas.* **31** 1203–16

Jensen L A, Onyskiw J E and Prasad N G N 1998 Meta-analysis of arterial oxygen saturation monitoring by pulse oximetry in adults *Heart Lung: J. Acute Crit. Care* **27** 387–408

Johansson A and Oberg P A 1999 Estimation of respiratory volumes from the photoplethysmographic signal. Part I: experimental results *Med. Biol. Eng. Comput.* **37** 42–7

Johnston W S and Mendelson Y 2004 Extracting breathing rate information from a wearable reflectance pulse oximeter sensor *IEEE Eng. Med. Biol. Soc.* **2** 5388–91 (https://ieeexplore.ieee.org/document/1404504)

Karlen W, Raman S, Ansermino J M and Dumont G A 2013 Multiparameter respiratory rate estimation from the photoplethysmogram *IEEE Trans. Biomed. Eng.* **60** 1946–53

Lázaro J, Gil E, Bailón R, Mincholé A and Laguna P 2013 Deriving respiration from photoplethysmographic pulse width *Med. Biol. Eng. Comput.* **51** 233–42

Lázaro J, Alcaine A, Romero D, Gil E, Laguna P, Pueyo E and Bailón R 2014a Electrocardiogram derived respiratory rate from QRS slopes and R-wave angle *Ann. Biomed. Eng.* **40** 2072–83

Lázaro J, Bailón R, Laguna P, Nam Y, Chon K and Gil E 2014b Respiratory rate influence in the resulting magnitude of pulse photoplethysmogram derived respiration signals *Proc. XLI Int. Conf. Computing in Cardiology* pp 289–92 (https://ieeexplore.ieee.org/stamp/stamp.jsp?tp=&arnumber=7043036)

Lin Y D, Ho H Y, Tsai C C, Wang S F, Lin K P and Chang H H 2013 Simultaneous heartbeat and respiration monitoring using PPG and RIIV on a smaprtphone device *Biomed. Eng. App. Basis Commun.* **25** 135–41

Meredith D J, Clifton D, Charlton P, Brooks J, Pugh C W and Tarassenko L 2012 Photoplethysmographic derivation of respiratory rate: a review of relevant physiology *J. Med. Eng. Technol.* **36** 1–7

Nilsson L, Johansson A and Kalman S 2000 Monitoring of respiratory rate in postoperative care using a new photoplethysmographic technique *J. Clin. Monit.* **16** 309–15

Nilsson L, Goscinski T, Kalman S, Lindberg L G and Johansson A 2007 Combined photoplethysmographic monitoring of respiration rate and pulse: a comparison between different measurement sites in spontaneously breathing subjects *Acta Anaesthesiologica Scand.* **51** 1250–7

Nitzan M, Babchenko A, Khanokh B and Landau D 1998 The variability of the photoplethysmographic signal—a potential method for the evaluation of the autonomic nervous system *Physiol. Meas.* **19** 93–102

Peralta E, Lázaro J, Bailón R, Marozas V and Gil E 2019 Optimal fiducial points for pulse rate variability analysis from forehead and finger PPG signals *Physiol. Meas.* **40** 025007

Pfurtscheller G, Schwarz G and Schwerdtfeger A 2018 Heart rate variability and impact of central pacemaker on cardiac activity *Clin. Neurophysiol.* **129** 2188–90

Seymour C W, Khan J M, Cooke C R, Watkins T R, Heckbert S R and Tea T D 2010 Prediction of critical illness during out-of-hospital emergency care *JAMA* **304** 747–54

Shelley K H 2007 Photoplethysmography: beyond the calculation of arterial oxygen saturation and heart rate *Anesthesia Analgesia* **105** S31–6

Sun S, Peeters W H, Bezemer R, Long X, Paulussen I, Aarts R M and Noordergraaf G J 2019 Finger and forehead photoplethysmography-derived pulse-pressure variation and the benefits of baseline correction *J. Clin. Monit. Comput.* **33** 65–75

Takazawa K, Tanaka N, Fujita M, Matsuoka O, Saiki T, Aikawa M, Tamura S and Ibukiyama C 1998 Assessment of vasoactive agents and vascular ageing by the second derivative of photoplethysmogram waveform *Hypertension* **32** 365–70